Dalton Transactions

ROYAL SOCIETY OF CHEMISTRY

PAPER

View Article Online
View Journal | View Issue

Cite this: *Dalton Trans.*, 2025, **54**, 16106

Catalytic degradation of *N*-acyl-homoserine lactone using a copper complex of a TACN derivative: implications for quorum sensing interference

Denisa Skurková, †[a,b] Hanna Zhukouskaya,†[a,c] Michaela Buziková,[d] Andrii Mahun,[a] Lívia Kanizsová,[a] Miroslav Vetrík,[a] Jan Kotek,[d] Martin Hrubý *[a] and Tomáš Tobrman*[c]

Medical treatment of bacterial biofilms represents a significant challenge, not only in the case of implant-associated infections but also in chronic inflammation of soft tissues. Therefore, further research is crucial to develop strategies that prevent biofilm formation at early stages, where quorum sensing (QS) signalling molecules that facilitate bacterial communication play a key role. In this study, we investigated the catalytic properties of an *N*-substituted triazacyclononane-copper(II) complex (Cu(II)-*i*Pr$_2$TACN), which mimicked the enzymatic activity of an acylase in the hydrolysis reaction of *N*-acyl-homoserine lactone (AHL), disrupting the QS in the bacterial biofilm as a result. Specifically, we focused on kinetic experiments involving the degradation of newly developed model AHLs with an acyl group derived from azobenzene as a chromophore label, enabling UV-VIS detection. ESI-MS was employed to identify the degradation products. Our results demonstrated sufficient hydrolytic activity against the model signalling molecules within relatively short time intervals under body temperature, blood pH and inflammation site conditions, with disruption occurring *via* lactone ring cleavage followed by further hydrolysis of the acyl fragment of the amide. To our knowledge, this is the first use of such complexes to degrade quorum sensing molecules. In addition, a novel UV-VIS active azodye chromophore-containing model substrate of a quorum sensing molecule was established for quorum quenching degradation studies and critically compared to other natural and synthetic quorum sensing molecules.

Received 9th July 2025,
Accepted 29th September 2025

DOI: 10.1039/d5dt01612f

rsc.li/dalton

Introduction

Bacterial biofilms are defined as structured communities of microorganisms (microcolonies) that adhere to biological or abiotic surfaces and are encased within a matrix of extracellular polymeric substances (EPSs).[1] The latter are secreted by attached cells and mainly include structural proteins (30–60%), polysaccharides (40–50%), DNA (2–5%), RNA (<5%) and other compounds, providing resistance to host immune response, physical removal, and antibiotic treatment.[2] Such biofilm-forming bacteria exhibit enhanced resistance to environmental stresses, including desiccation, UV radiation, metal toxicity, and light exposure.[3] Biofilm development progresses through distinct stages: initial reversible and irreversible attachment to surfaces, growth, maturation, and eventual dispersion. Dispersed bacteria can colonise nearby tissues and establish new biofilm communities. A key mechanism governing biofilm formation is quorum sensing (QS), which enables bacterial communication through population density-dependent signalling.

Most bacterial and fungal species can form biofilms to survive. The use of antibiotics continues to be the primary approach in the treatment of infectious diseases. However, it has been established that bacteria in the form of biofilms demonstrate up to a 1000-fold increase in resistance to antibiotic treatment, making them hard to eradicate. Biofilm resistance mechanisms, such as reduced metabolic activity, altered microenvironment and increased efflux pumps, contribute to a higher rate of mutations. Strategies to fight bacterial biofilm-

[a]*Institute of Macromolecular Chemistry, Czech Academy of Sciences, Heyrovského náměstí 2, 162 00 Prague 6, Czech Republic. E-mail: mhruby@centrum.cz; Tel: +420296 809 130*
[b]*Department of Organic Chemistry, Faculty of Chemistry and Technology, University of Chemistry and Technology, Prague, Technická 5, 166 28 Prague 6, Czech Republic*
[c]*Department of Physical and Macromolecular Chemistry, Faculty of Science, Charles University, Hlavova 8, Prague, 128 43, Czech Republic. E-mail: tomas.tobrman@vscht.cz; Tel: +420 220 444 245*
[d]*Department of Inorganic Chemistry, Charles, University, Hlavova 8, 128 40 Prague 2, Czech Republic*
† These authors contributed equally to this article.

associated infections include therapies combining antibiotics, immunomodulators and entities causing various mechanisms of quorum quenching (QQ).[4,5] The development of bioactive molecules is a key area in drug discovery, and this strategy is now also applied to identify compounds that disrupt quorum sensing and biofilm formation.[6]

Biofilm-associated infections pose a significant clinical challenge due to the ability of bacteria to form structured communities within a self-produced matrix, increasing antibiotic resistance and evading host immune responses. More than 65% of bacterial infections involve biofilm formation, making it a prevalent issue in infection processes.[7] Medical devices, such as catheters and prosthetics, are particularly susceptible to biofilm colonisation, often leading to persistent, difficult-to-treat infections.[8] Biofilms are also implicated in non-device-associated infections, such as native valve endocarditis and chronic sinusitis. The primary obstacle in treating biofilm-associated infections is their high resistance to conventional antibiotics, primarily due to the protective nature of the biofilm matrix and the altered metabolism of the bacteria.

N-Acyl-homoserine lactones (AHLs) in Gram-negative bacteria and autoinducing peptides in Gram-positive bacteria are central to QS.[2,9] These molecules regulate bacterial behaviour, including biofilm formation, virulence, competence, and sporulation. For instance, *Pseudomonas aeruginosa* starts to form biofilms in response to high cell density caused by the accumulation of autoinducers, while *Vibrio cholerae* and *Staphylococcus aureus* begin biofilm formation at low cell density, as the autoinducer build-up inhibits this process.[10] Once released, autoinducers accumulate in the extracellular space, and upon reaching a critical threshold, they are detected by specialised bacterial receptors, triggering a cascade of signalling pathways that regulate biofilm formation and other related processes. This sophisticated intercellular communication plays a crucial role in the coordination of bacterial activities and adaptation to changing environments.[11] The AHLs, used by Gram-negative bacteria, consist of a lactone ring with an acyl chain ranging from 4 to 18 carbons in length, substituted at the third position, which can be unmodified or feature an oxo or a hydroxyl group. The integrity of the lactone ring is crucial for the molecule's immunoactive properties. The stability of AHL molecules, specifically of their lactone ring, can be affected by environmental conditions, such as pH and temperature. Under alkaline conditions, the lactone can hydrolyse, leading to a loss of signalling activity. The relationship between pH and lactone ring stability is given by the expression $1/(1 \times 10^7\ [OH^-])$, which represents the half-life of the lactone ring in days.[10] For instance, at pH 7, the homoserine lactone ring can remain stable for several hours, while at pH 8.5, its stability decreases to tens of minutes. The effect of temperature on lactone hydrolysis is quantified through the temperature coefficient, indicating that for each 1 °C increase, the hydrolysis rate will grow by a factor of 1.03 to 1.08, depending on the acyl chain length of the AHL.[12]

The communication between bacteria can also be disrupted in several ways (Fig. 1). One of the possibilities is enzymatic

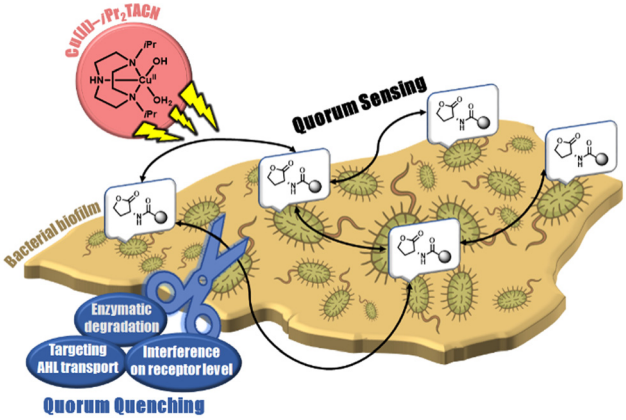

Fig. 1 Overview of QQ strategies.

QQ. This can be done by acylases, which cleave the amide bond of AHLs, or lactonases and hydrolyse the lactone ring, thereby inactivating the signalling molecules.[13] Another promising approach to the disruption of QS includes antibodies that specifically bind to the signalling molecules, preventing them from interacting with the corresponding bacterial receptors. Janda *et al.* made a significant contribution in this area by developing the anti-AHL antibody RS2-1G9, which was produced in response to the synthetic 3-oxo-AHL analogue RS2. This antibody effectively inhibited quorum sensing *in vitro* in *Pseudomonas aeruginosa* by capturing the signalling molecule 3-oxo-C12-HSL.[14] Both natural and synthetic QS inhibitors have demonstrated their effectiveness in quorum quenching, with examples including vanillin, malic and lactic acids, lemongrass and citrus extracts, cinnamaldehyde, 4-nitropyridine-*N*-oxide, and many others.[15]

The synthesis of molecules mimicking enzymatic activity is an attractive reference in the field of bacterial biofilm research. There are four key features central to the action of natural enzymes and their artificial analogues, namely transition-state stabilisation, pseudo-intramolecular reactions, functional group positioning, and microenvironment modulation. By using these principles, several catalysts functioning as enzyme mimics have been developed. These include natural molecules, such as cyclodextrins and catalytic antibodies, as well as complex synthetic systems, *e.g.*, functional macrocycles, imprinted polymers, and dendrimers.[16] Additionally, self-assembling nanosystems, such as soft micellar and vesicular aggregates, and solid nanoparticles, have also been studied. Complexes of transition metal ions, *e.g.* Cu(II) and Zn(II), are known to act as active homo- and heterogeneous catalysts of hydrolysis reactions, capable of cleaving, *e.g.*, phosphate ester or amide bonds with significant rate enhancement and good recyclability. Similar catalytic behaviour is also observed in transition metal oxide surfaces, which are active in oxidation reactions and are increasingly investigated within applied surface science.[17] TACN represents a 9-membered aza-crown ether, which coordinates the metal ion in a tridentate fashion.[18] The main reason for using TACN derivatives is that

their complexes are coordinatively unsaturated.[19] The TACN ligand ensures the copper(II) ions remain in solution at all pH values and temperatures, with two adjacent coordination sites on copper(II) being free and exposed for catalysis. The ligand also decreases the toxicity of copper toward eukaryotic cells to negligible values compared to that of free copper. The action of the TACN derivatives involves water activation, nucleophilic attack and transition state stabilisation.[20] These complexes function as artificial nucleases, capable of cleaving the stable phosphodiester bonds in bacterial DNA, thereby preventing biofilm formation.[21–25] Among the wide array of ligands and metals tested for such applications, copper(II) complexes of TACN and its derivatives stand out as particularly efficient catalysts.[26] For instance, silica-bound copper(II)-TACN materials show hydrolytic properties toward phosphate esters.[27] In our previous work, we investigated a series of TACN ligands and their copper(II) complexes for their ability to hydrolyse phosphodiester bonds, using bis(4-nitrophenyl)phosphate (BNPP) as a model substrate. The study included both simple TACN ligands and more complex derivatives with functionalised side arms designed for potential incorporation into polymeric materials. Among the complexes, copper(II)-1,4-diisopropyl-1,4,7-triazacyclononane (Cu(II)-*i*Pr$_2$TACN) exhibited the highest hydrolytic activity while maintaining full water solubility of both the free ligand and the complex.[28] The hydrolytic activity was retained after immobilisation, as demonstrated by the hydrolysis of toxic organophosphate.[29] Non-coordinating isopropyl groups were chosen as they represent a balanced compromise: they are sufficiently sterically demanding to effectively suppress the formation of the hydrolytically inactive dimer, while at the same time are not overly hydrophobic. Therefore, their employment allows the ligand to be conveniently handled in aqueous solution during complex formation. Their non-coordinating nature is particularly important to ensure that two coordination sites on the central metal atom remain available for the binding of the substrate and the hydroxide, as these are essential for the hydrolysis to proceed.

According to literature data, copper(II) complexes are the most active in such cases. In our previous work, we also tested Mg(II) and Zn(II) complexes, which showed significantly lower catalytic efficiency. The Ni(II) complex was not tested, as the ion is very toxic and has negligible potential for *in vivo* use. Furthermore, the exchange kinetics of simple ligands on the Ni(II) complexes are usually much slower than that for ligands on the Cu(II) complexes, *e.g.*, for the exchange of water molecules, the process is about five orders of magnitude faster for Cu(II) over Ni(II) aquacomplexes.[20,30]

Given that acyl-homoserine lactones (AHLs, Fig. 2), which are key molecules in bacterial quorum sensing and biofilm formation, feature a potentially hydrolytically cleavable lactone functional group, we anticipated that copper(II)-TACN complexes might also target and disrupt these signalling molecules to achieve quorum quenching and suppress biofilm formation in this way. To test this hypothesis, we selected Cu(II)-*i*Pr$_2$TACN for its proven catalytic efficiency in different systems. The azo-dye-chromophore-containing model *N*-acyl-homoserine lactone (MAHL) was newly synthesised as a model compound, containing the hydrophobic non-charged chromophore, which facilitates detection of reaction progress. Besides this new compound, the hydrolyses of commercially available naturally occurring *N*-phenylacetyl-L-homoserine lactone (NAHL) and synthetic *N*-benzyloxycarbonyl-L-homoserine lactone (SAHL) were studied for comparison.

High-performance liquid chromatography combined with diode array UV-VIS detection and mass spectrometry analysis using electrospray ionisation coupled with quadrupole ion trap detection was employed to monitor the reactions and to determine the kinetic parameters of its degradation. Our findings demonstrated that the studied Cu(II)-*i*Pr$_2$TACN complex could be a promising candidate for quorum quenching applications, potentially offering a viable strategy to prevent the formation of biofilms on medical devices. To the best of our knowledge, this is the first use of such complexes to degrade quorum sensing molecules. In addition, we established a novel UV-VIS-active model substrate containing an azobenzene chromophore to mimic quorum sensing molecules, enabling quorum quenching degradation studies and critical comparison with natural and synthetic quorum sensing molecules.

Materials and methods

Reagents and materials

3-(4-Aminophenyl)propionic acid, anhydrous *N*,*N*-dimethylformamide (DMF), *N*,*N*-dimethylaniline, 4-(*N*,*N*-dimethylamino)pyridine (DMAP), *N*,*N*-diisopropylethylamine (DIPEA), benzotriazol-1-yloxytripyrrolidinophosphonium hexafluorophosphate (PyBOP), $NaNO_2$ and CH_3CO_2Na were purchased from Sigma-Aldrich Ltd (Prague, Czech Republic). L-Homoserine lactone hydrochloride, *N*-phenylacetyl-L-homoserine lactone (NAHL) and *N*-carbobenzoxy-L-homoserine

Fig. 2 The general formula of *N*-acyl-homoserine lactones (AHLs) used by bacteria for quorum sensing and the formulas of the studied compounds.

lactone (SAHL) were purchased from Cayman Chemical (Ann Arbor, MI, USA). Immobilized penicillin G acylase was obtained from Biosynth (Bratislava, Slovakia). The ligand *i*Pr$_2$TACN and the complex Cu(II)-*i*Pr$_2$TACN were prepared according to the literature.[31]

Characterisation and purification

Flash chromatography. Products were isolated using a puriFlash XS 420 chromatography system (Interchim; Montluçon, France) using original columns (PF-30-SIHP-JP-F0080, spherical silica, particle size: 30 μm) with UV detection at 254 and 280 nm.

Nuclear magnetic resonance (NMR) spectroscopy. The ^{1}H NMR spectra were recorded at 25 °C on a Bruker Avance III 600 spectrometer (Bruker; Billerica, MA, USA) operating at 600.13 MHz. Samples were prepared in deuterated solvents. The spectra were acquired using a 90° pulse (width = 18 μs) with a recycle delay of 10 s and 64 scans. Chemical shifts δ are given in ppm and coupling constants J in Hz. The chemical shifts were calibrated relative to TMS using hexamethyldisiloxane (HMDSO, 0.05 ppm from TMS in the ^{1}H spectra) as an external standard. All NMR spectra were processed using Bruker TopSpin 4.5.0 software.

Fourier transform infrared spectroscopy with attenuated total reflectance (ATR-FTIR). The ATR-FTIR measurements of the samples were performed using a Nexus 870 FTIR spectrometer (Thermo Nicolet; Madison, WI, USA) equipped with a mercury cadmium telluride detector and a universal ATR accessory with a diamond prism. The spectra were averaged over 256 scans at a resolution of 4 cm^{-1}.

Electrospray ionisation or matrix-assisted laser desorption/ionisation-time of flight mass spectrometry (ESI-MS; MALDI-TOF). ESI-MS mass spectrometry measurements for establishing the molecular mass of compounds were conducted on an LCQ Fleet mass analyser with electrospray ionisation (Thermo Fisher Scientific; Waltham, MA, USA).

MALDI-TOF mass spectrometry was performed on an ultrafleXtreme TOF–TOF instrument (Bruker Daltonics, Germany) equipped with a 2000 Hz smartbeam-II laser (355 nm), operated in positive-ion reflectron mode with panoramic pulsed ion extraction. Samples were prepared using the dried droplet method with Milli-Q water (Milli-Q® IQ 7000, Merck) as the solvent, mixed with 2,5-dihydroxybenzoic acid (20 mg mL^{-1}) as the matrix and NaCl (10 mg mL^{-1}) as the ionising agent in a 4 : 20 : 1 volume ratio. External calibration was used. More details can be found in the SI.

Ultra-high-performance liquid chromatography (UHPLC). Precise chromatography measurements were carried out on a Dionex UltiMate 3000 UHPLC system (Thermo Fisher Scientific; Waltham, MA, USA) equipped with an RS pump module, a diode array detector (200/256/360/650 nm), and a fluorescence detector (fluorescence traces are not used). A Chromolith HighResolution RP18-e column with a water/acetonitrile eluent gradient (95% H_2O/4.9% acetonitrile (ACN)/0.1% trifluoroacetic acid (TFA) to 5% H_2O/94.9% ACN/0.1% TFA in 15 min) with a flow rate of 1 mL min^{-1} was used. The gradient method consisted of (0.0–0.5 min): isocratic phase at 95% H_2O/5% ACN (equilibration); 0.5–8.5 min: linear gradient to 5% H_2O/95% ACN (separation); 8.5–9.8 min: isocratic phase at 5% H_2O/95% ACN (column wash); 9.8–10 min (return to initial conditions).

Synthesis of the *N*-acyl-homoserine lactone azo dye model

Synthesis of the azo dye chromophore (ADC). The synthesis was performed by a modified procedure from the one reported in the literature,[31] as shown in Scheme 1. To a solution of 3-(4-aminophenyl)propanoic acid (0.57 g, 3.5 mmol, 1.0 eq.) in 1 M HCl (7 mL, 2 eq.), 2.5 M $NaNO_2$ (0.36 g, 5.22 mmol, 1.5 eq., dissolved in 2.1 mL H_2O) was added dropwise while the reaction mixture was cooled to 0 °C in an ice bath. The mixture was subsequently stirred for 1 h. A solution of *N*,*N*-dimethylaniline (0.54 mL, 4.3 mmol, 1.2 eq.) in a mixture of AcOH (10 mL) and H_2O (5 mL) was then added to the cooled mixture, followed by stirring at 0 °C for the next 3 h. The pH was adjusted to 4 using 2 M sodium acetate, resulting in a precipitate that was collected by filtration, washed with cold water and diethyl ether, and dried under vacuum. The product, 3-(4-((4-(dimethylamino)phenyl)diazenyl)phenyl)propanoic acid (ADC), was obtained as a dark orange solid (0.78 g, 2.63 mmol, 75%).

NMR (600 MHz, DMSO-d_6): ^{1}H δ 12.14 (*s*, 1H), 7.77 (*d*, J = 9.01, 2H), 7.69 (*d*, J = 8.23, 2H), 7.37 (*d*, J = 8.23, 2H), 6.83 (*d*, J = 9.0, 2H), 3.05 (*s*, 6H), 2.89 (*t*, J = 7.60, 2H), 2.58 (*t*, J = 7.60, 2H). ^{13}C{^{1}H} δ 174.2, 152.9, 151.4, 143.3, 143.1, 129.6, 125.1, 122.3, 112.1, 40.6, 35.5, 30.6. Detailed NMR characterisation is stated in Fig. S1–S4.

FT-IR: ν(–CH$_2$–) = 2917 cm^{-1}, ν(N(CH$_3$)$_2$) = 2855–2800 cm^{-1}, ν(O–H) = 2624–2544 cm^{-1}, ν(C=O) = 1702 cm^{-1}, δ(aromatic C–H) = 1599 cm^{-1}, ν(N=N) = 1517 cm^{-1}, ν(aromatic ring) = 1424 cm^{-1}, ν(N(CH$_3$)$_2$) = 1366 cm^{-1}, ν(C=O) = 1300 cm^{-1}, ν(amine C–N) = 1214–1137 cm^{-1}, δ(aromatic C–H) = 945 and 818 cm^{-1}, δ(aromatic ring) = 676 cm^{-1}. The FT-IR, MALDI-TOF, ESI-MS and UHPLC data are shown in Fig. S5–S8.

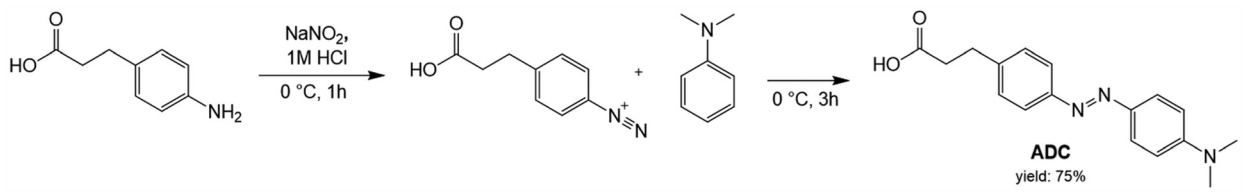

Scheme 1 Synthetic scheme of the ADC (azo dye chromophore).

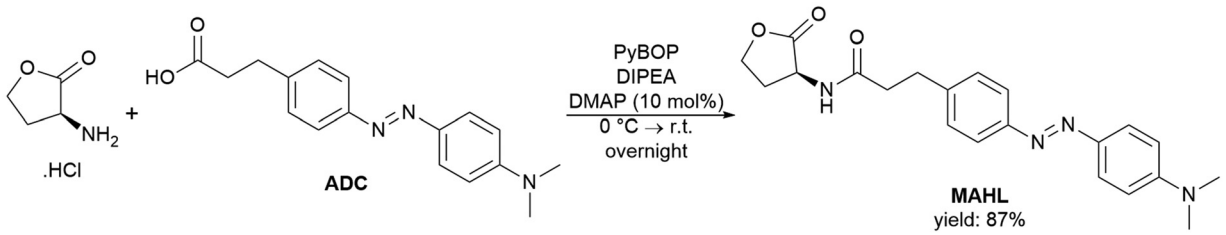

Scheme 2 Synthetic scheme of the MAHL (model *N*-acyl-homoserine lactone).

Synthesis of the *N*-acyl-homoserine lactone (MAHL) model. The synthesis was performed according to Scheme 2.

A solution of ADC (0.25 g, 0.84 mmol, 1.0 eq.) in DMF (2 mL) was combined with PyBOP (0.49 g, 0.94 mmol, 1.1 eq.), DIPEA (0.33 mL, 1.89 mmol, 2.25 eq.) and a catalytic amount of DMAP (0.01 g, 10 mol%), and the mixture was cooled to 0 °C in an ice bath. To this activated carboxylic acid mixture, a solution of L-homoserine lactone hydrochloride (0.15 g, 1.1 mmol, 1.3 eq.) and DIPEA (0.19 mL, 1.1 mmol, 1.3 eq.) in 0.5 mL DMF was added. The reaction was allowed to warm to room temperature and stirred overnight. The mixture was concentrated under reduced pressure, and the residue was dried under vacuum. Purification by flash chromatography with a 95 : 5 (cyclohexane : ethyl acetate) mobile phase afforded MAHL as a dark orange solid (0.28 g, 0.74 mmol, 87%).

NMR (400 MHz, DMSO-d_6): ^{1}H δ 8.41 (d, J = 8.0, 1H), 7.77 (d, J = 8.8, 2H), 7.69 (d, J = 8.1, 2H), 7.36 (d, J = 8.0, 2H), 6.82 (d, J = 8.8, 2H), 4.54 (dt, J = 10.9, 8.5, 1H), 4.34 (td, J = 8.8, 1.9, 1H), 4.20 (td, J = 10.5, 8.7, 1H), 3.05 (s, 6H), 2.89 (t, J = 7.6, 2H), 2.46 (td, J = 7.60, 2.99, 2H), 2.37 (m, J = 9.20), 2.10 (m, J = 10.6, 1H). ^{13}C{^{1}H} δ 175.8, 171.9, 152.9, 151.4, 143.5, 143.1, 129.6, 125.1, 122.3, 112.1, 65.8, 48.4, 40.6, 37.0, 31.2, 28.8. Detailed NMR characterisation is stated in Fig. S9–S13.

FT-IR: ν(N–H) = 3301 cm^{-1}, ν(–CH$_2$–) = 2925 cm^{-1}, ν(N(CH$_3$)$_2$) = 2855–2800 cm^{-1}, ν(lactone C=O) = 1777 cm^{-1}, ν(amide C=O) = 1644 cm^{-1}, δ(aromatic C–H) = 1600 cm^{-1}, ν(amide C–N) = 1547 cm^{-1}, ν(N=N) = 1516 cm^{-1}, ν(aromatic ring) = 1444 cm^{-1}, ν(N(CH$_3$)$_2$) = 1361 cm^{-1}, ν(amine C–N) = 1223–1140 cm^{-1}, δ(aromatic C–H) = 1012 and 820 cm^{-1}, δ(N–H) = 772 cm^{-1}. The FT-IR, MALDI-TOF, ESI-MS and UHPLC data are shown in Fig. S14–S16 and S8.

Cu(II)-*i*Pr$_2$TACN-catalysed degradation studies

UHPLC measurement of degradation kinetics. UHPLC was used to study the hydrolysis of MAHL. Unfortunately, in the case of NAHL (see Fig. S17 and S18) and SAHL, the method cannot be successfully used due to the weak light absorption of the compounds and their hydrolytic products and the UHPLC peak overlay with the catalyst. All chemicals used in the study were of analytical grade. Buffers were prepared using MilliQ water, with MES used for pH values of 5.0 and 6.5, and TRIS for pH 7.4. The concentration of the buffers was 150 mM. The pH adjustments were made using 1M HCl for TRIS buffers and 2M NaOH for MES buffers, measured using a pH meter from Eitech Instruments (a part of Thermo Fisher Scientific) with an accuracy of ±0.01 pH units. Due to the low solubility of MAHL in pure buffers, a 1 : 1 (v/v) mixture of MES/TRIS and acetonitrile was used to prepare 10 mM stock solutions. For MAHL (M = 380.44 g mol^{-1}), 3.80 mg was used to prepare 1 mL of 10 mM stock solution in TRIS/MES buffer : ACN (1 : 1, v/v). The concentration of the aqueous stock solution of Cu(II)-*i*Pr$_2$TACN was 10 mM. Stabilities of the stock solutions of MAHL were studied in individual buffers (pH = 5.0, 6.5, and 7.4) and 50 °C to obtain insight into degradation under the chosen experimental conditions. For details, see the SI (Fig. S19).

Reaction mixtures for degradation studies were prepared by mixing 0.10 mL of buffered 10 mM MAHL solution with 0.90 mL of 10 mM Cu(II)-*i*Pr$_2$TACN solution to obtain a final MAHL concentration of 1 mM and a Cu(II)-*i*Pr$_2$TACN concentration of 9 mM. Reaction mixtures were incubated at the corresponding temperature for five minutes before the first UHPLC measurement. Aliquots of 20 μL were taken at predefined time intervals (0, 0.5, 1, 2, 5, 24, 48 h, and up to 5 days) and diluted with 40 μL of phase A (H$_2$O/ACN/TFA; 95/5/0.1) of the UHPLC mobile phase before analysis.

The degradation of MAHL (t_r = 6.5 min, m/z = 381.28, [M + H]$^+$) was monitored, together with the appearance of products at t_r = 5.7 (1st hydrolysis product, m/z = 399.30, [M + H]$^+$) and 5.2 min (2nd hydrolysis product, ADC, m/z = 298.19, [M + H]$^+$). The degradation products were analysed by ESI-MS (see the SI).

To obtain at least preliminary data also for Cu(II)-*i*Pr$_2$TACN-mediated hydrolysis of NAHL (M = 219.20 g mol^{-1}), 2.19 mg was used to prepare 1 mL of 10 mM stock solution. The hydrolytic reaction was performed in the same way as described above for MAHL; the chosen representative conditions were pH 7.4 and 50 °C. The decrease in peak intensity of NAHL (t_r = 4.7 min) was followed, and two new emerging peaks at t_r = 4.2 (1st hydrolysis product) and 3.6 min (2nd hydrolysis product) gradually appeared. The degradation product standards were prepared by alkaline (1st hydrolysis product) and acid (2nd hydrolysis product, phenylacetic acid) hydrolyses, and their identity was confirmed by UHPLC and MALDI-TOF. For details, see the SI (Scheme S1 and Fig. S20, S21).

^{1}H NMR measurement of degradation kinetics. ^{1}H NMR spectroscopy was used to study the hydrolysis of NAHL (see Fig. S22) and SAHL; unfortunately, in the case of MAHL, the

method cannot give reliable results due to the low solubility of MAHL and its hydrolytic products in buffered D_2O : acetonitrile-d_6 solvent and complicated overlay of the signals. For details, see the SI (Fig. S23).

All NMR kinetic experiments were carried out at 50 °C, maintaining the "pH" to 7.4; the term "pH" means a direct (uncorrected) electrode reading in a D_2O : ACN-d_6 mixture. Deuterated solvents were employed to minimise ^{1}H NMR spectral interference. A TRIS buffer solution (150 mM) was prepared by dissolving 50 mg of TRIS base (M = 121.14 g mol^{-1}) in a mixture of 1.5 mL deuterium oxide (D_2O) and 1.5 mL of deuterated acetonitrile (ACN-d_6). The apparent pH was adjusted using deuterated hydrochloric acid (HCl-d_1) to 7.4. A 15 mM solution of Cu(II)-*i*Pr$_2$TACN in deuterated buffer was prepared by evaporating 4.50 mL of an aqueous 10 mM Cu(II)-*i*Pr$_2$TACN stock solution using a vacuum rotary evaporator. The dry residue was re-dissolved in 3.00 mL of the previously prepared buffer (TRIS : ACN-d_6 1 : 1 v/v). Solutions of AHLs were prepared at a concentration of 15 mM by dissolving the corresponding compounds in the buffer (TRIS : ACN-d_6 1 : 1 v/v). Specifically, 3.29 mg of NAHL (M = 219.24 g mol^{-1}) and 3.53 mg of SAHL (M = 235.24 g mol^{-1}) were each dissolved in 1 mL of the buffer.

Reaction mixtures were prepared by combining 0.190 mL of the 15 mM AHL stock solution with 0.380 mL of the 15 mM Cu(II)-*i*Pr$_2$TACN stock solution in the NMR tube. This corresponds to a 1 : 2 molar ratio of AHL to Cu(II)-*i*Pr$_2$TACN. The degradation studies were conducted at 50 °C for 5 h. The NMR spectra were recorded at regular intervals, with measurements taken every 10 min during the first hour and every 30 min thereafter. The standards of the degradation products of SAHL were prepared by alkaline (1st hydrolysis product) and acid (2nd hydrolysis product, benzyl alcohol) hydrolysis and characterised by ^{1}H NMR (Scheme S2 and Fig. S24–S26).

Enzyme-catalysed degradation studies. Enzyme-catalysed degradation studies were carried out using immobilised penicillin G acylase (PGA), a commercially available enzyme widely employed in the pharmaceutical industry for the production of semi-synthetic β-lactam antibiotics. Based on the established protocol, optimal reaction conditions for the enzyme were set – pH 8.0 and 28 °C – with an enzymatic activity of 240 U g^{-1} for the immobilised form. This setup enabled a comparative evaluation between the natural enzymatic degradation of MAHL and NAHL and the newly developed Cu(II)-*i*Pr$_2$TACN-catalysed hydrolysis.

For the enzymatic degradation experiments, 1 mL of a 10 mM MAHL or NAHL solution was prepared by following the same procedure used for the UHPLC kinetic analysis. To ensure detection of even minimal hydrolytic activity, 20.8 mg of immobilised PGA – providing approximately 5 U of enzymatic activity – was used for NAHL. The samples were gently mixed and incubated at 28 °C and pH 8. After 5 min of pre-incubation, the first UHPLC measurement was conducted. Aliquots of 20 μL were collected at defined time points (0 h, 24 h and 48 h) and diluted with 40 μL of mobile phase A (H_2O/ACN/TFA; 95/5/0.1) before analysis.

The appearance of the degradation products was monitored by UHPLC, with the appearance of the new peaks at t_r = 5.6 and 5.3 min corresponding to the hydrolytic products of MAHL, and t_r = 4.2 and 3.6 min corresponding to the hydrolytic products of NAHL, respectively. The resulting peaks were analysed by MS to ensure that the products of enzyme-catalysed hydrolysis are the same as those of Cu(II)-*i*Pr$_2$TACN-catalysed hydrolysis.

Results

This study was focused on several types of AHLs (Fig. 2) to investigate their degradation kinetics under different pH (5.0, 6.5 and 7.4) and temperature (23, 37 and 50 °C) conditions. A new model AHL (MAHL) was designed and synthesised as a compound containing an azo-dye chromophore system (Schemes 1 and 2), which allowed us to follow the reaction kinetics using UHPLC and UV-VIS detection. *In vivo*, the actual concentrations of *N*-acyl-homoserine lactones are very low in surrounding body fluids, typically in the picomolar to nanomolar range, although they can reach micromolar levels within the biofilm matrix itself. In contrast, the formal concentration of the complex in close proximity to the modified surface during potential *in vivo* application will be high due to the small volume. The real concentrations of AHL in biofilms are even lower than those we used (we used the lowest concentration readily appropriate for the analyses employed), so the real AHL-to-catalyst ratio could be even much lower.

Alongside MAHL, two additional AHLs were included to examine how structural differences influence degradation patterns. NAHL (*N*-phenylacetyl-L-homoserine lactone) is a natural quorum sensing agent commonly observed during Gram-negative bacterial biofilm formation. SAHL (*N*-carbobenzoxy-L-homoserine lactone), a synthetic AHL featuring a carbamate functional group, was also studied to explore how non-natural modifications to the AHL structure influence degradation kinetics and potential quorum quenching activity. Using UHPLC and ^{1}H NMR, the degradation kinetics of MAHL, NAHL, and SAHL in the presence of the Cu(II)-*i*Pr$_2$TACN complex were successfully tracked. Additionally, MAHL and NAHL were tested with enzymatic catalysis using penicillin G acylase (PGA) to provide qualitative insights into the biomimetic properties of the Cu(II)-*i*Pr$_2$TACN complex. This approach provided a reliable and straightforward method for monitoring the degradation process directly, without requiring derivatisation or additional adjustments to the detection system.

Spontaneous degradation of MAHL followed by UHPLC

The intermediate in MAHL synthesis, ADC, was found to be fully stable under the conditions used, as would be expected from its chemical structure – indeed, no changes in UHPLC traces were observed upon standing the stock solutions in buffers at 50 °C for several days. However, for MAHL, spontaneous hydrolysis of the lactone ring and/or amide bond can be expected. The UHPLC measurement showed that MAHL (t_r

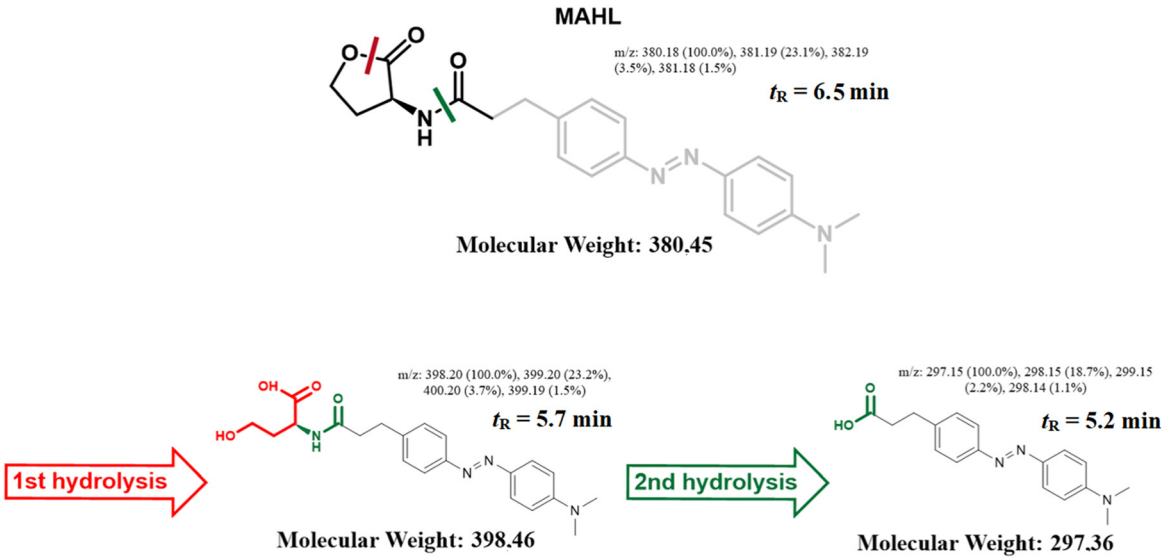

Scheme 3 Subsequent hydrolysis of the MAHL.

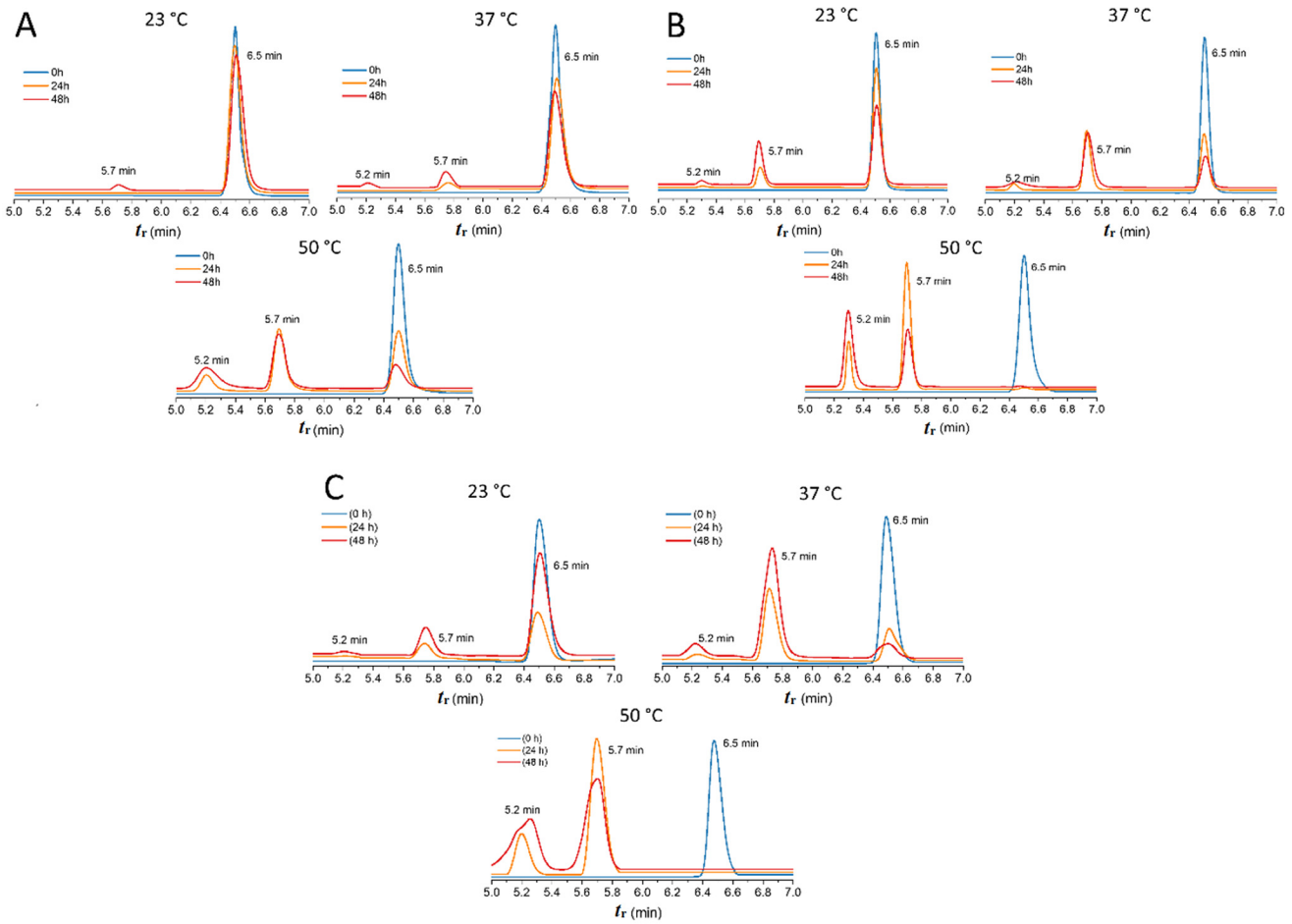

Fig. 3 UHPLC chromatograms of MAHL hydrolysis catalysed by the Cu(II)-*i*Pr$_2$TACN complex at different temperatures (23, 37 and 50 °C) and constant pH values: pH 5.0 (A), pH 6.5 (B) and pH 7.4 (C).

= 6.5 min) was found to be fully stable at pH 5.0 and 50 °C over two days, but at pH 6.5 and 7.4, some slow degradation was observed. At pH 6.5, about 10% of MAHL was transformed after 48 h into a new compound with t_r = 5.7 min, identified by MS as the product of lactone ring opening (1st hydrolysis), and at pH 7.4, about 30% of MAHL was degraded, affording *ca.* 25% of the product of the 1st hydrolysis and 5% of ADC (2nd hydrolysis, t_r = 5.2 min); see Fig. S19. Thus, the subsequent hydrolytic pathway as shown in Scheme 3 can be suggested. Controls for all three temperatures and all three pH values were tested. Observable spontaneous non-catalyzed hydrolysis was observed only at pH 7.4 and 50 °C and is presented in Fig. S18 and S19. The spontaneous hydrolysis was slower by approximately an order of magnitude and, thus, it was neglected in the catalytic studies. Moreover, for potential use, total hydrolysis rates are important and, therefore, the total hydrolysis rate values are stated in the manuscript.

Cu(II)-*i*Pr$_2$TACN-mediated degradation of MAHL and NAHL followed by UHPLC

The MAHL hydrolysis performed in the presence of the Cu(II)-*i*Pr$_2$TACN complex proceeds much faster than the spontaneous hydrolysis discussed above. The product of the lactone ring opening (UHPLC peak at t_r = 5.7 min) was detected after just 0.5 h. Over time, the product of the 2nd hydrolysis starts to be form (t_r = 5.2 min). At 50 °C and pH 5.0, MAHL is converted into hydrolytic products from *ca.* 80% after 48 h, and at pH 6.5 and 7.4, it is fully hydrolysed even after 24 h under these conditions. Representative UHPLC chromatograms are shown in Fig. 3.

To quantify the kinetics of MAHL hydrolysis, we analysed UHPLC peak areas at specific reaction times. We applied a pseudo-first-order kinetics model, which is justified by the fact that water and Cu(II)-*i*Pr$_2$TACN are present in high excess and can be considered constant. As a result, changes in the reaction rate could be reasonably attributed to the concentration of MAHL alone, thus simplifying the analysis. This approach has also been commonly used in related metal-catalysed AHL hydrolysis studies, including zinc-based systems.[32] Semilogarithmic data linearization using the pseudo-first-order model provided very good linearity and, thus, the apparent rate constant can be easily evaluated as the slope of the linear regression (Fig. 4). The observed rate constant and corresponding degradation half-life values are summarised in Table 1.

These results demonstrate that MAHL degradation is strongly pH- and temperature-dependent. An increase in temp-

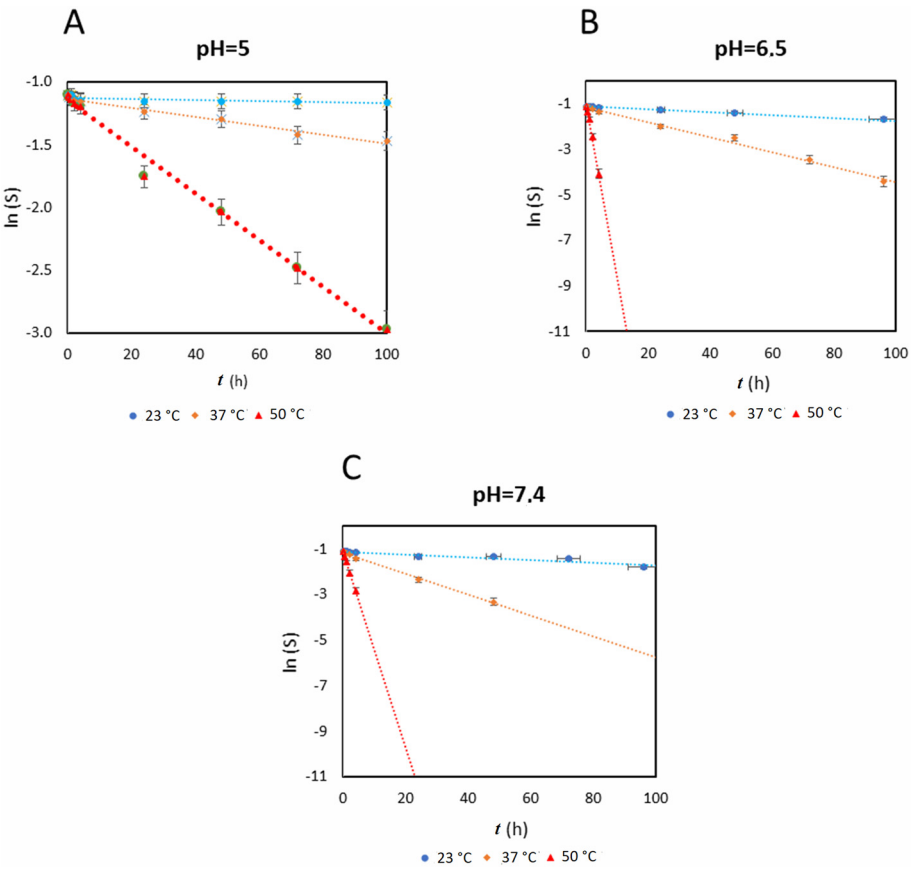

Fig. 4 Kinetic curves of catalysed MAHL decomposition by the Cu(II)-*i*Pr$_2$TACN complex, plotted in semilogarithmic coordinates at various temperatures and pH values, using 0.15 M MES (A and B) and 0.15 M TRIS (C) buffers. ln(S) is the logarithm of the area under the peak on the UHPLC chromatogram.

Table 1 The observed rate constants (h^{-1}) and half-lifes (h) of MAHL decomposition catalysed by the Cu(II)-*i*Pr$_2$TACN complex under different conditions

pH	5			6.5			7.4		
T (°C)	23	37	50	23	37	50	23	37	50
k_{obs} (h^{-1})	4.0×10^{-4}	3.6×10^{-3}	1.9×10^{-2}	6.7×10^{-3}	3.3×10^{-2}	0.76	6.1×10^{-3}	4.6×10^{-2}	0.43
$t_{\frac{1}{2}}$ (h)	1.7×10^{3}	1.9×10^{2}	37	104	21	0.90	114	15	1.6

erature of *ca.* 15 °C results in an increase of the rate constant by approximately one order of magnitude. At pH 5.0, the hydrolysis is at its slowest, and much faster degradation was observed at pH 6.5 and 7.4. Moreover, at these pH values, the hydrolysis rates are comparable.

To generalise the ability of Cu(II)-*i*Pr$_2$TACN to mediate AHL hydrolysis, NAHL was hydrolysed at 50 °C and pH 7.4 under analogous conditions to those used for MAHL (concentrations, buffer, and time points). Although integration of the UHPLC peaks is somewhat difficult in this case (low intensity of absorption leading to a relatively poor baseline), the rate constant of 0.27 h^{-1} ($t_{\frac{1}{2}}$ = 2.6 h) can be evaluated from the data.

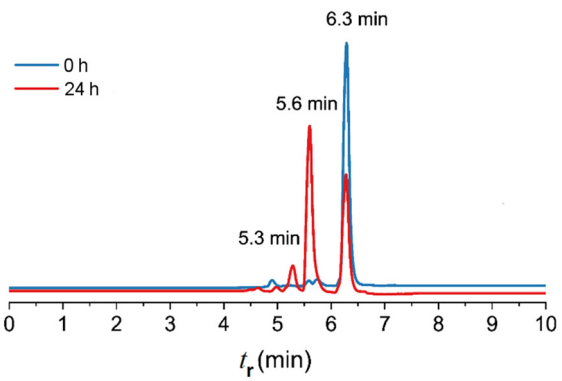

Fig. 5 UHPLC chromatograms of the enzymatic degradation of MAHL at 28 °C and pH 8 in 0.15 M TRIS.

Enzymatic degradation of MAHL and NAHL followed by UHPLC

Hydrolysis of MAHL and NAHL with penicillin G acylase (PGA) was also performed for comparison, as this enzyme, widely employed in the industrial production of semi-synthetic penicillin, is well known for its high efficiency and specificity in amide bond hydrolysis. For maximum enzymatic activity and substrate conversion, the experiments were carried out under optimal conditions of the enzyme as established in previous studies (pH 8, 28 °C).

Upon testing MAHL with PGA at its full enzymatic strength, 240 U, we observed the formation of the expected degradation products, as shown in Fig. 5, with retention times of 5.6 and 5.3 minutes. These products are the same as those observed in MAHL spontaneous hydrolysis and during hydrolysis mediated by Cu(II)-*i*Pr$_2$TACN. This finding confirmed that the enzyme-catalysed hydrolysis occurred as anticipated.

To ensure that hydrolysis of NAHL is promoted specifically by the enzyme and not merely by the presence of water, or heating conditions, a stability test of NAHL under the same conditions as the experiment was performed (MES buffer, pH 8, 28 °C). As shown in Fig. 6A, no degradation occurred after 24 h. On the other hand, the emergence of the 1st hydrolytic product at t_r = 4.2 min and the 2nd hydrolytic product at t_r = 3.6 min after 24 h is clearly seen in Fig. 6B for the enzyme-catalysed reaction.

To confirm the expected products of degradation, standards of the expected 1st and 2nd hydrolysis products were prepared by hydrolysis (Scheme S1). The 1st hydrolytic product was

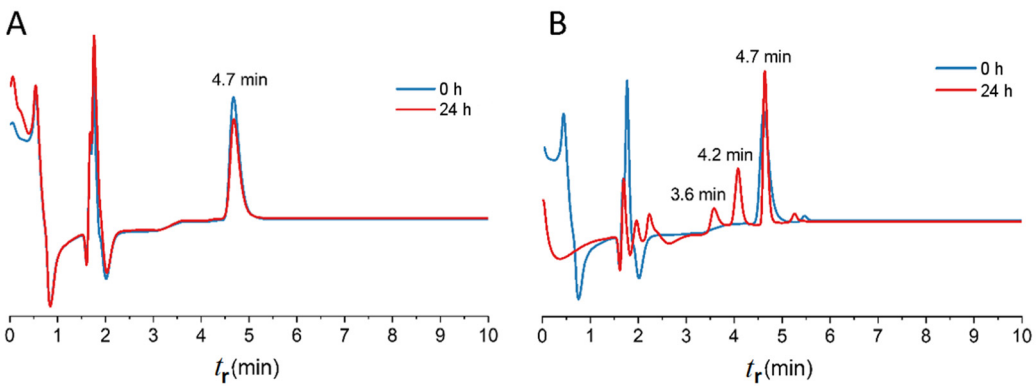

Fig. 6 UHPLC curves of NAHL: (A) stability in buffer solution without enzyme and (B) enzymatic decomposition at a constant temperature of 28 °C and a constant pH value of 8.

obtained by alkaline lactone ring opening by treating NAHL with dilute NaOH and heating at 50 °C. UHPLC analysis showed a peak at t_r = 4.2 min (Fig. S17), and MALDI-TOF MS was used for confirmation (Fig. S18). A portion of the same mixture was then acidified and re-heated, yielding two peaks by UHPLC: one at t_r = 4.7 min (back formation of NAHL by lactone ring reformation in acidic media), and another at t_r = 3.6 min, corresponding to phenylacetic acid (product of the 2nd hydrolysis), which was confirmed by MALDI-TOF MS and GC-MS after trimethylsilylation (Fig. S21).

The experiments revealed a consistent trend in AHL hydrolysis – in all cases (spontaneous, enzymatically promoted and Cu(II)-*i*Pr$_2$TACN-mediated), the lactone ring opening occurs first, followed by the amide bond splitting.

Cu(II)-*i*Pr$_2$TACN-mediated degradation of NAHL and SAHL followed by ^{1}H NMR

For NMR spectroscopy, our initial attempts employed the AHL : Cu(II)-complex 1 : 9 molar ratio as used in the UHPLC studies. However, this setup resulted in poor spectral resolution due to the concentration of AHL being insufficient and the presence of large paramagnetic effects of the Cu(II)-complex, making it unsuitable for reliable analyses. To address this, we adjusted the ratio to 1 : 2, achieved by mixing 0.38 mL of 15 mM AHL with 0.19 mL of 15 mM Cu(II)-*i*Pr$_2$TACN. This provided final concentrations of 1.5 mM AHL and 3 mM Cu(II)-*i*Pr$_2$TACN. The revised 1 : 2 ratio in the NMR experiments ensured that enough AHL was present for detection while minimising spectral interference from excess Cu(II)-*i*Pr$_2$TACN. This balance was critical for maintaining clear and interpretable spectra.

In contrast to the UHPLC conditions – where MAHL was readily soluble in a 1 : 1 (v/v) MES/TRIS buffer and acetonitrile mixture at a 1 : 9 molar ratio with Cu(II)-*i*Pr$_2$TACN – the ^{1}H NMR experiments employed deuterated solvents (TRIS : ACN-d_6, 1 : 1 v/v) and a lower Cu(II)-*i*Pr$_2$TACN excess (1 : 2 molar ratio), under which MAHL exhibited poor solubility, resulting in low-intensity signals and poorly resolved NMR spectra that precluded meaningful kinetic analysis.

For NAHL, hydrolysis was indicated by the appearance of signals in the aromatic region of the ^{1}H NMR spectrum (7.5–8 ppm, Fig. 7B). The decomposition was tracked by a decrease in the intensity of signals "1 + 2" and "6" (Fig. 7A). Due to overlapping peaks, it is challenging to determine whether the second hydrolysis product was formed, as its signals will overlap with those from NAHL and the first product. It probably occurs and causes the slightly non-linear nature of the kinetic data (Fig. 9, red dots).

The same approach was applied to investigate the hydrolysis of SAHL. Formation of the product from the first hydrolysis step was identified. Although most of the NMR signals from SAHL and its product overlap with each other and with solvent signals, a distinct peak at 5.45 ppm (labelled 4′ in Fig. 8A) was observed. This signal corresponds to the Ar–C*H*$_2$–

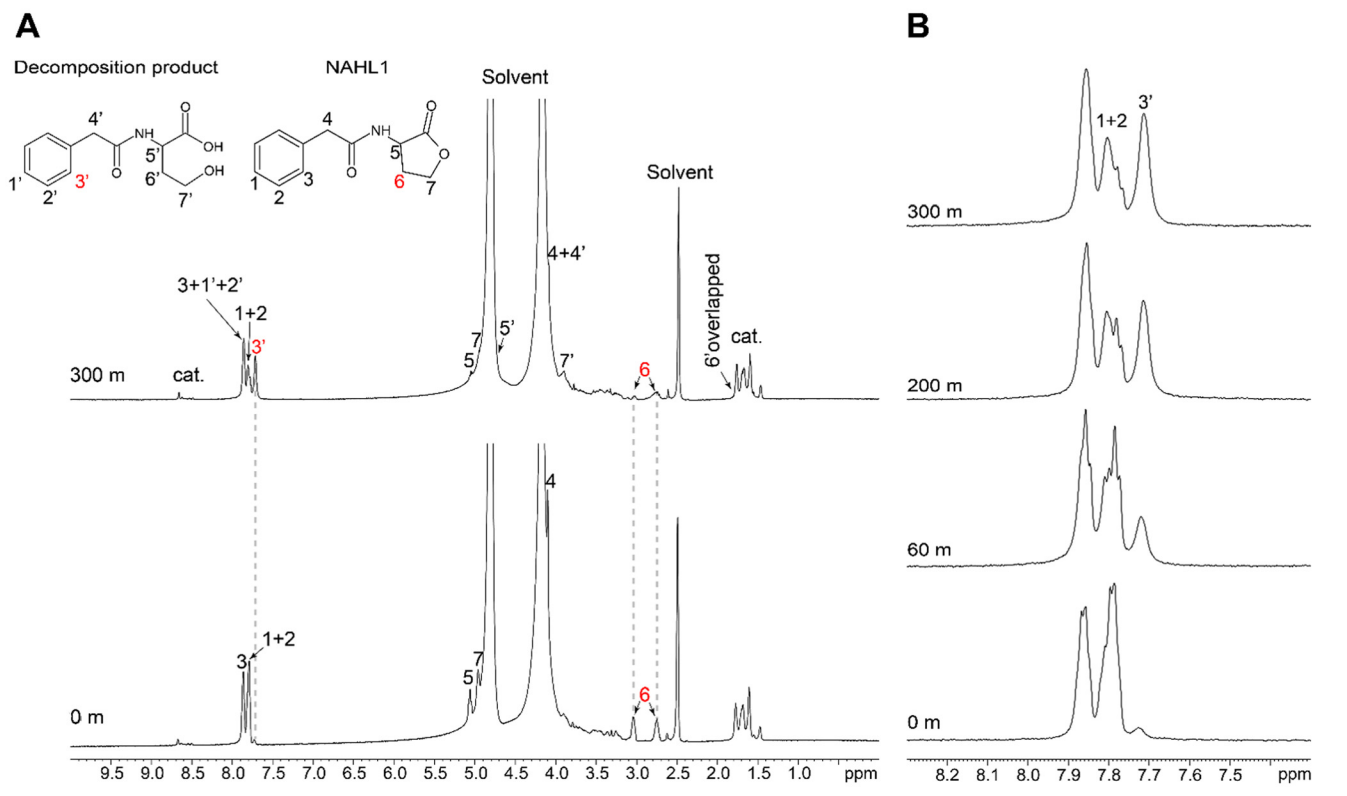

Fig. 7 (A) Degradation of NAHL in the presence of Cu(II)-*i*Pr$_2$TACN as followed by ^{1}H NMR. (B) Close-up of the aromatic peaks followed for kinetics.

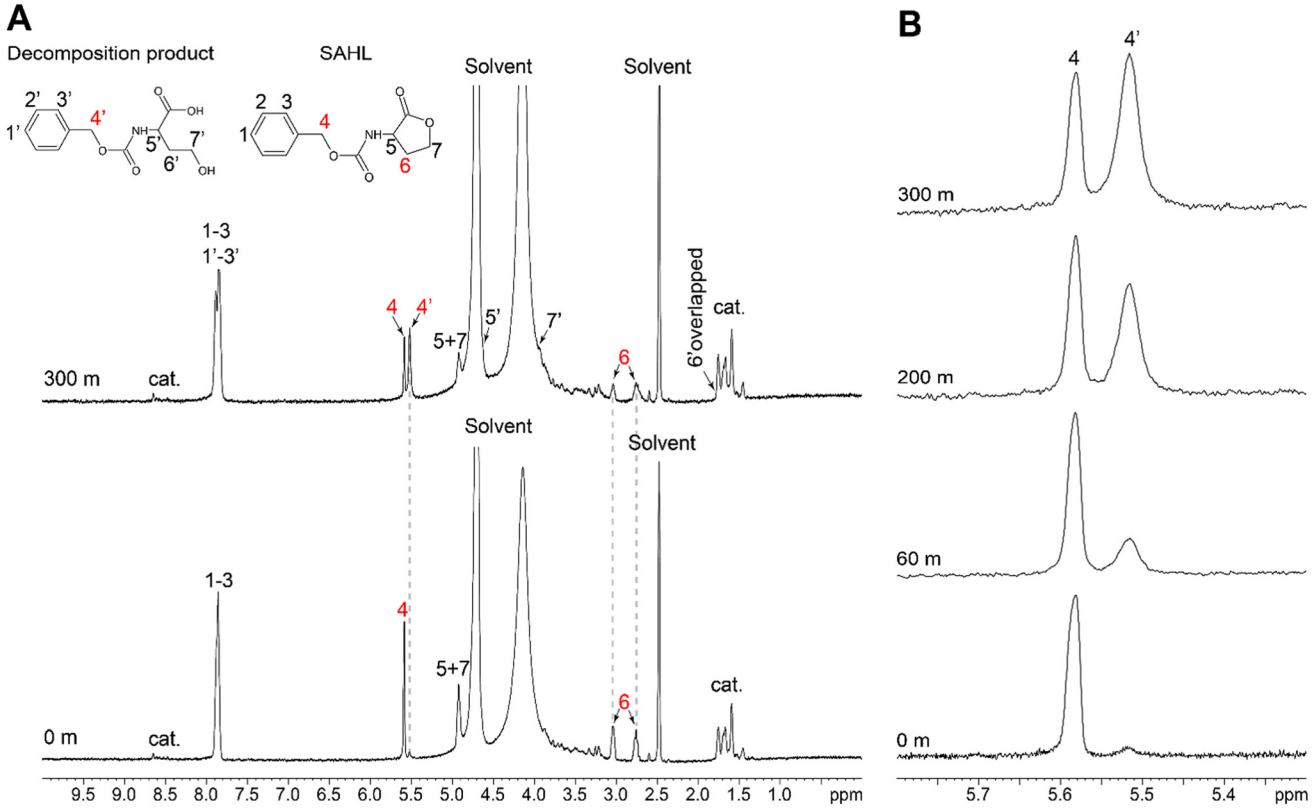

Fig. 8 (A) Degradation of SAHL in the presence of Cu(II)-*i*Pr$_2$TACN as followed by ^{1}H NMR. (B) Close-up of the peaks followed for kinetics.

O– protons of the hydrolysis product. Its increasing intensity was monitored (Fig. 8B) alongside the decreasing intensity of the corresponding SAHL signal (labelled 4) and the lactone ring signal (labelled 6). Under the given experimental conditions, no visible production of CO_2 gas was observed in the cuvette; however, due to CO_2 solubility in aqueous media, it cannot be concluded if the 2nd hydrolytic step occurred or not. For details, see Fig. S25.

These data were used to construct a kinetic profile for NAHL and SAHL (Fig. 9A). The red line represents the decomposition of NAHL, yielding a kinetic rate constant of k_{obs} = 0.26 h^{-1} and $t_{\frac{1}{2}}$ = 2.7 h. Nevertheless, the non-linear

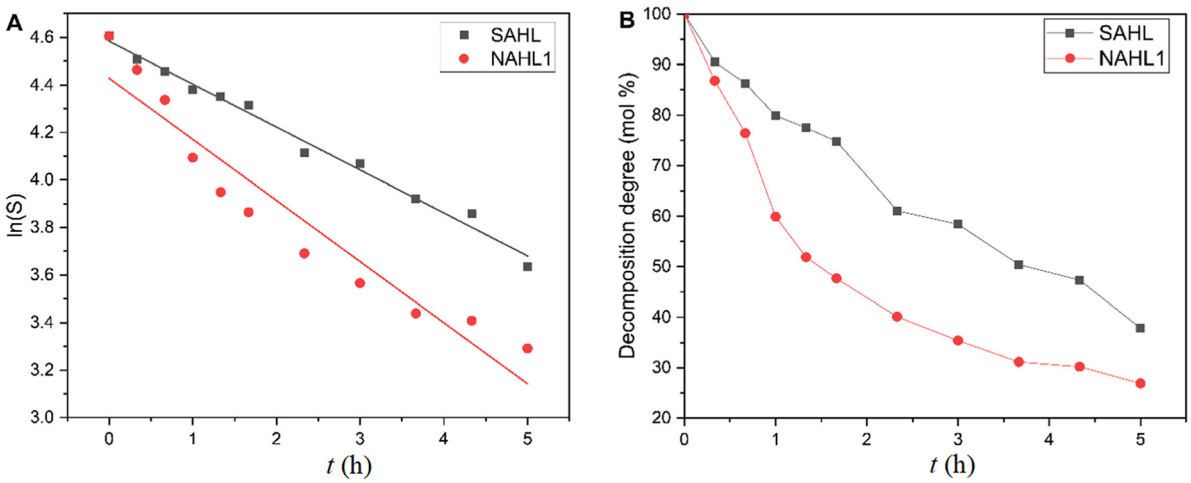

Fig. 9 (A) Pseudo-first order kinetics of catalysed degradation of NAHL (red) and SAHL (black) decomposition and (B) relative decrease of the concentrations of NAHL (red) and SAHL (grey) as followed by ^{1}H NMR measurements (for (B), the lines connecting points have no physical meaning and are just guides for the eye).

nature of the kinetic data suggests the possibility of a two-stage decomposition process with distinct kinetic rates for the subsequent NAHL decomposition.

Decomposition of SAHL shows better linearity (black line) than that of NAHL, yielding a kinetic rate constant of k_{obs} = 0.18 h^{-1}, corresponding to $t_{\frac{1}{2}}$ = 3.8 h. Under the given experimental conditions, the formation of the second hydrolysis product cannot be confirmed or disproved. Although no visible production of CO_2 gas was observed in the cuvette, the sample had a low concentration, and CO_2 has good solubility in aqueous media.

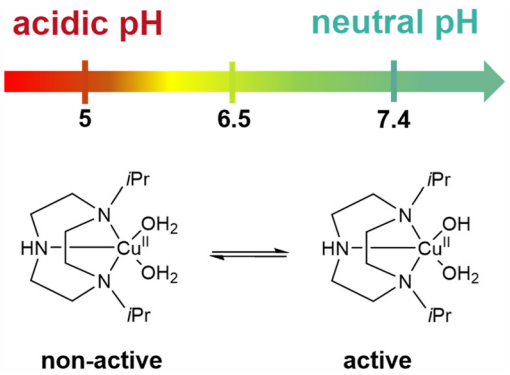

Fig. 10 The pH-dependent behaviour of Cu(II)-*i*Pr$_2$TACN and its impact on hydrolysis kinetics.

Discussion

Impact of pH on the kinetics of MAHL hydrolysis mediated by Cu(II)-*i*Pr$_2$TACN

The degradation of MAHL using Cu(II)-*i*Pr$_2$TACN was strongly influenced by pH and temperature. Faster degradation was observed at elevated temperatures and around neutral pH (similar kinetic values were obtained at pH 6.5 and 7.4), under which the full degradation proceeded rapidly within ~<10 h. At body temperature (37 °C), the degradation of MAHL using Cu(II)-*i*Pr$_2$TACN showed comparable degradation half-life values at pH 7.4, representing blood and extracellular fluid, as well as at pH 6.5, typical of inflammation sites – 15 and 21 h, respectively. In contrast, at pH 5, the degradation half-life extended significantly to 190 h. These observations (including data from all temperatures) point to a saturation character of the rate constant with increasing pH. This supports the commonly suggested mechanism that the formation of hydroxido-complex species is crucial for efficient catalysis. At pH 5, the predominant diaqua species $[Cu(iPr_2TACN)(H_2O)_2]^{2+}$ results in significantly reduced catalytic efficiency due to the poor nucleophilicity of coordinated water. The highest activity is

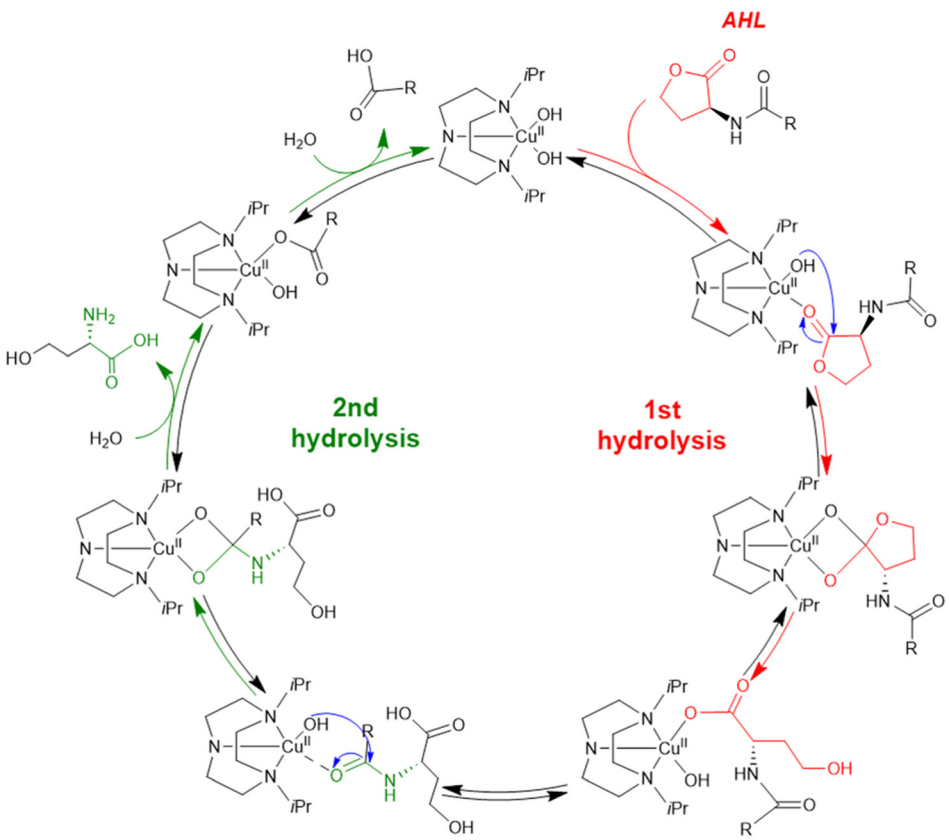

Fig. 11 Proposed mechanism for the hydrolysis of *N*-acyl-homoserine lactones by Cu(II)-*i*Pr$_2$TACN.

observed at pH 6.5–7.4, where the formation of the monohydroxo species $[Cu(iPr_2TACN)(OH)(H_2O)]^+$ enhances nucleophilicity while maintaining an electrophilic Cu(II) centre for substrate activation (Fig. 10). In general, the TACN derivatives form stable complexes, which are well-known to have two other coordination places occupied by additional ligands, typically by water molecules. The "acidity" constants of the coordinated water molecule were determined for several derivatives (TACN itself, trimethyl or tris(isopropyl) derivatives, and other related compounds; see ref. 21–25), and lie in the range of pH 7.5–8.0.

Therefore, the overall mechanism of AHL hydrolysis can be suggested as shown in Fig. 11.

The suggested mechanism is proposed as occurring *via* a two-step process: initial lactone ring hydrolysis followed by amide bond cleavage. Although the precise reaction pathway has not been fully studied, this mechanism is supported by the observed degradation products of MAHL and parallels the generally accepted Cu(II)-*i*Pr$_2$TACN-based hydrolytic reaction mechanism, particularly for phosphate ester hydrolysis.

These results further support the versatility of Cu(II)-*i*Pr$_2$TACN in degrading both natural and synthetic AHLs, offering a wider range of action in comparison with the enzymatic approach while achieving comparable outcomes in terms of expected degradation products. In summary, the Cu(II)-*i*Pr$_2$TACN complex demonstrates superior efficiency and versatility as a catalytic agent, offering significant advantages over traditional enzymatic methods for QQ and biofilm control.

Degradation of MAHL, NAHL and SAHL with Cu(II)-*i*Pr$_2$TACN

Based on ESI-MS analysis, lactone ring opening occurs as the first degradation step, followed by slower amide bond hydrolysis. All studied AHLs show comparable degradation rates in the presence of the Cu(II)-*i*Pr$_2$TACN complex, as demonstrated by the data compiled in Table 2. The negligible effect of aqueous or deuterated media on the hydrolytic reaction suggests that the reaction mechanism does not depend on proton transfer and fully supports that the crucial step is the transfer of the hydroxido group, as suggested in the mechanistic scheme shown in Fig. 11. Steric hindrance in the vicinity of the cleaved bonds in the substrate can be considered to influence the hydrolysis rate. MAHL, showing the fastest hydrolysis, has lower steric hindrance of the lactone ring (acyl group being –CO–CH$_2$–CH$_2$–Ar for MAHL compared to –CO–CH$_2$–Ar for NAHL). These results further support the versatility of Cu(II)-*i*Pr$_2$TACN in degrading both natural and synthetic AHLs, offering a wider range of action in comparison with the enzymatic approach while achieving comparable outcomes in terms of expected degradation products. In summary, the Cu(II)-*i*Pr$_2$TACN complex demonstrates superior efficiency and versatility as a catalytic agent, offering significant advantages over traditional enzymatic methods for QQ and biofilm control.

Table 2 Half-lifes (h) and other data of catalysed MAHL, NAHL and SAHL decomposition by Cu(II)-*i*Pr$_2$TACN at pH 7.4 and 50 °C

AHL	k_{obs} (h^{-1})	$t_{\frac{1}{2}}$ (h)
MAHL[a]	0.43	1.6
NAHL[a]	0.27	2.6
NAHL[b]	0.26	2.7
SAHL[b]	0.18	3.7

[a] Obtained by UHPLC. [b] Obtained by ^{1}H NMR.

Conclusions

This study presents the catalytic potential of the *N*-substituted 1,4,7-triazacyclononane copper complex (Cu(II)-*i*Pr$_2$TACN) in degrading quorum sensing signalling molecules, specifically *N*-acyl-homoserine lactones (AHLs), the communicating agents of Gram-negative bacteria. The findings obtained demonstrate the ability of Cu(II)-*i*Pr$_2$TACN to efficiently hydrolyse AHLs under physiological and pathological conditions, thereby disrupting quorum sensing and inhibiting bacterial biofilm formation. This mechanism mirrors enzymatic activity while offering advantages in reaction kinetics and operational stability, as evidenced by the significant degradation observed under body temperature and pH conditions representative of blood and inflammation sites. Our research highlights the versatility of the Cu(II)-*i*Pr$_2$TACN complex in degrading both natural and synthetic AHLs, with kinetic studies revealing its effectiveness across a range of environmental conditions. Moreover, comparison with enzymatic approaches, such as that involving penicillin G acylase, underlines the superior speed and comparable outcomes of Cu(II)-*i*Pr$_2$TACN-based catalysis. These results underscore the promise of Cu(II)-*i*Pr$_2$TACN as a robust and scalable tool for quorum quenching and biofilm control, with potential applications in combating antibiotic-resistant bacterial infections and enhancing the longevity of medical devices. Future work should focus on further optimising the design of copper(II)-TACN complexes to enhance their catalytic efficiency, biocompatibility, and integration into practical antimicrobial coatings or therapies. The Cu(II)-*i*Pr$_2$TACN complex also demonstrates notable biomimetic potential by replicating key catalytic features of natural metalloenzymes, such as water activation, intermediate stabilisation, and lactone ring hydrolysis. However, it is important to acknowledge that natural metalloenzymatic systems are highly complex biological entities, involving intricate networks of structural and functional components. Cu(II)-*i*Pr$_2$TACN mimics only specific aspects of these systems, particularly their catalytic core while lacking the broader biological sophistication of enzymes. Nonetheless, its ability to emulate these critical enzymatic functions while offering superior operational stability and broader substrate versatility underscores its value as a biomimetic tool for disrupting quorum sensing and addressing biofilm-associated challenges. This research also emphasises the urgent need to develop innovative strategies to combat the rising threat of antibiotic resistance, which poses a significant global health challenge. With biofilm-associated infections often displaying heightened re-

sistance to conventional antibiotics, quorum quenching strategies such as those enabled by Cu(II)-*i*Pr$_2$TACN represent a promising avenue, as shown in this model study. The development of alternative approaches to target bacterial communication and biofilm formation is critical for overcoming the limitations of traditional antibiotics and mitigating the escalating burden of resistant bacterial infections.

Author contributions

Conceptualization: M. H. and J. K.; methodology: M. V., J. K., and M. H.; validation: D. S., H. Z., M. B., M. V., J. K., M. H., and L. K.; formal analysis: D. S., H. Z., J. K., and L. K.; investigation: D. S., H. Z., M. B., A. M., and M. V.; data curation: D. S. and H. Z.; writing – original draft preparation: D. S., H. Z., and M. H.; writing – review and editing: M. H., J. K., M. B. and T. T.; visualization: D. S. and H. Z.; supervision: M. H., M. V., J. K., and T. T.; project administration: M. H.; funding acquisition: M. H.

Conflicts of interest

The authors declare no conflicts of interest. The funders had no role in the design of the study, in the collection, analyses, or interpretation of data, in the writing of the manuscript, or in the decision to publish the results.

Data availability

The data supporting this article have been included as part of the supplementary information (SI). Supplementary information is available. See DOI: https://doi.org/10.1039/d5dt01612f.

Acknowledgements

This research was funded by the Ministry of Education, Youth and Sports of the Czech Republic (grants # INTER-ACTION LUAUS24272 and LM2023053 ERIC). This study was co-funded by the project New Technologies for Translational Research in Pharmaceutical Sciences/NETPHARM, project ID CZ.02.01.01/00/22_008/0004607, co-funded by the European Union.

References

1 A. Zhao, J. Sun and Y. Liu, *Front. Cell. Infect. Microbiol.*, 2023, **13**, 1137947.
2 R. Srinivasan, S. Santhakumari, P. Poonguzhali, M. Geetha, M. Dyavaiah and L. Xiangmin, *Front. Microbiol.*, 2021, **12**(12), 676458.
3 A. Vertes, V. Hitchins and K. S. Phillips, *Anal. Chem.*, 2012, **84**, 3858–3866.
4 X. Wang, M. Liu, C. Yu, J. Li and X. Zhou, *Mol. Biomed.*, 2023, **4**, 49.
5 H. Y. Liu, E. L. Prentice and M. A. Webber, *npj Antimicrob. Resist.*, 2024, **2**, 27.
6 Q. Q. Lu, Y. M. Chen, H. R. Liu, J. Y. Yan, P. W. Cui, Q. F. Zhang, X. H. Gao, X. Feng and Y. Z. Liu, *Drug Dev. Res.*, 2020, **81**, 1037–1047.
7 M.-B. Huang, D. Brena, J. Y. Wu, M. Shelton and V. C. Bond, *Microbiol. Spectrum*, 2024, **12**, 2.
8 A. Shariati, S. Vesal, A. Khoshbayan, P. Goudarzi, D. Darban-Sarokhalil, S. Razavi, M. Didehdar and Z. Chegini, *J. Appl. Microbiol.*, 2022, **132**, 2531–2546.
9 G. Coquant, J.-P. Grill and P. Seksik, *Front. Immunol.*, 2020, **11**, 1827.
10 S. Mukherjee and B. L. Bassler, *Nat. Rev. Microbiol.*, 2019, **17**, 371–382.
11 A. R. Horswill, P. Stoodley, P. S. Stewart and M. R. Parsek, *Anal. Bioanal. Chem.*, 2007, **387**, 371–380.
12 C. C. Roggatz and D. R. Parsons, *Front. Mar. Sci.*, 2022, **9**, 882428.
13 Y.-C. Wang, C. Wang, M.-F. Han, Z. Tong, X.-R. Hu, Y.-T. Lin and X. Zhao, *Chemosphere*, 2022, **288**, 132465.
14 N. Amara, B. P. Krom, G. F. Kaufmann and M. M. Meijler, *Chem. Rev.*, 2011, **111**, 195–208.
15 G. Scarascia, T. Wang and P. Y. Hong, *Antibiotics*, 2016, **5**, 39.
16 Y. Lyu and P. Scrimin, *ACS Catal.*, 2021, **11**, 11501–11509.
17 Y. Sun, Y. Zhu, T. Xin, X. Li, X. Zhou, G. Bai, W. Chang and R. Zhu, *Appl. Surf. Sci.*, 2025, **708**, 163768.
18 E. Macedi, A. Bencini, C. Caltagirone and V. Lippolis, *Coord. Chem. Rev.*, 2020, **407**, 213151.
19 P. Chaudhuri and K. Wieghardt, The chemistry of 1,4,7-triazacyclononane and related tridentate macrocyclic compounds, in *Progress in Inorganic Chemistry*, ed. S. J. Lippard, Wiley, New York, 1987, vol. 35, pp. 329–436, DOI: 10.1002/9780470166369.ch4.
20 E. L. Hegg and J. N. Burstyn, *Coord. Chem. Rev.*, 1998, **173**, 133–165.
21 K. M. Deck, T. A. Tseng and J. N. Burstyn, *Inorg. Chem.*, 2002, **41**, 669–677.
22 F. H. Fry, A. J. Fischmann, M. J. Belousoff, L. Spiccia and J. Brugger, *Inorg. Chem.*, 2005, **44**, 941–950.
23 L. Tjioe, T. Joshi, C. M. Forsyth, B. Moubaraki, K. S. Murray, J. Brugger, B. Graham and L. Spiccia, *Inorg. Chem.*, 2012, **51**, 939–953.
24 K. A. Deal and J. N. Burstyn, *Inorg. Chem.*, 1996, **35**, 2792–2798.
25 M. J. Belousoff, A. R. Battle, B. Graham and L. Spiccia, *Polyhedron*, 2007, **26**, 344–355.
26 D. Desbouis, I. P. Troitsky, M. J. Belousoff, L. Spiccia and B. Graham, *Coord. Chem. Rev.*, 2012, **256**, 897–937.
27 C. Ortega-Nieto, N. Losada-Garcia, D. Prodan, G. Furtos and J. M. Palomo, *Nanomaterials*, 2023, **13**, 2406.
28 M. Buziková, R. Willimetz and J. Kotek, *Molecules*, 2023, **28**, 7542.

29 M. Buziková, H. Zhukouskaya, E. Tomšík, M. Vetrík, J. Kučka, M. Hrubý and J. Kotek, *Polymers*, 2024, **16**, 2911.
30 L. Helm and A. E. Merbach, *Chem. Rev.*, 2005, **105**, 1923–1959, DOI: 10.1021/cr030726o.
31 Y. Nakajima, M. Kawaguchi, N. Ieda and H. Nakagawa, *ACS Med. Chem. Lett.*, 2021, **12**, 617–624.
32 R.-Z. Liao, J.-G. Yu and F. Himo, *Inorg. Chem.*, 2009, **48**, 1442–1448.